Connections between Meteor Persistent Trains and Ozone Content in the Mesosphere and Lower Thermosphere

L. E. Cordonnier[1,2], K. S. Obenberger[1], J. M. Holmes[1], G. B. Taylor[2], and D. Vida[3]

[1]Space Vehicles Directorate, Air Force Research Laboratory, Kirtland AFB, NM, USA
[2]Department of Physics and Astronomy, University of New Mexico, Albuquerque, NM, USA
[3]Department of Physics and Astronomy, University of Western Ontario, London, ON, Canada

Key Points:

- Seasonal ozone variations in the mesopause are strongly correlated with the occurrence rate of persistent trains left by sporadic meteors
- Meteor showers exhibit weaker ozone correlation, highlighting the importance of intrinsic meteoroid properties in forming persistent trains
- There are not any clear trends between ozone content and the duration of persistent trains

Corresponding author: Logan Cordonnier, `lcordonnier@unm.edu`

Abstract

Ozone (O_3) is an important trace species in the mesosphere and lower thermosphere (MLT) region. We found a strong correlation between the average peak O_3 volume mixing ratio (vmr) of the secondary ozone maximum (~90-95 km) and the percentage of sporadic meteors that produce persistent trains (PTs). PTs are long-lasting, self-emitting phenomena that occasionally form after a meteor, arising from exothermic reactions between meteoric metals and atmospheric O_3. The correlation between PTs and O_3 enables one to estimate the O_3 content by determining the fraction of sporadic meteors that left behind observable PTs. This represents a new, ground-based technique for estimating O_3 content in the upper atmosphere. Meteor showers were much less correlated with O_3 due to their respective homogeneity, stressing the importance of intrinsic meteoroid properties for PT formation. Lastly, we examined the connection between O_3 content and the duration of PTs and found no clear trend.

Plain Language Summary

Ozone (O_3) plays an important role in the atmosphere; there is a buildup of O_3 in the mesosphere and lower thermosphere region (at altitudes of 90-95 km) known as the secondary O_3 maximum. We have found that the amount of O_3 located in this secondary maximum is strongly correlated with the fraction of sporadic meteors (i.e. meteors not associated with any meteor shower) that leave behind observable persistent trains (PTs). PTs are glowing trails that some meteors leave behind which can last for several minutes up to an hour—their light is produced from chemical reactions between metals in the meteors and O_3 in the atmosphere. Because PTs and O_3 are strongly correlated, we can use the fraction of meteors with PTs to estimate how much O_3 is present. Meteor showers are worse at estimating O_3 because different meteor showers have different properties, which makes some showers particularly good or bad at making PTs. Lastly, we investigated whether the amount of O_3 has an effect on how long PTs last before they fade away; we did not find any convincing evidence to suggest that it does.

1 Introduction

Ozone (O_3), though a trace species, is an important component in the mesosphere-lower thermosphere (MLT) region from 70 to 120 km. MLT ozone is involved in a variety of processes—it contributes to atmospheric heating via absorption of solar ultraviolet radiation and is a participant in photochemical and exothermic reactions. It is a key constituent for the overall radiative, chemical, and energy budget of the MLT. In addition to the well-known stratospheric O_3 layer, a secondary maximum in O_3 concentration is found near the mesopause (~90-95 km) with a local minimum occurring at 80 km (Smith et al., 2013). O_3 in this secondary maximum arises due to the termolecular recombination of molecular (O_2) and atomic (O) oxygen with a third catalytic species (e.g. nitrogen); O is initially produced in the lower thermosphere from photolyzed O_2 (due to solar ultraviolet radiation), which is then transported downward into the MLT (Newnham et al., 2022). The global minimum in temperature at the mesopause contributes to the buildup of O_3 in this region, as low temperatures favor O_3 production and hinder reactions that destroy it (Smith & Marsh, 2005). It has been well-documented that the volume mixing ratio (vmr) of the secondary O_3 maximum exhibits diurnal variations (e.g. Vaughan, 1982; Rogers et al., 2009). In a simplified picture, the O_3 recombination process described above is opposed primarily by strong solar photolysis during the day and by destructive reactions with atomic hydrogen (H) at night, albeit to a lesser degree (Rogers et al., 2009). The nighttime ozone vmr is up to ~10 times larger than the daytime value because of this (Vaughan, 1982), though the relative magnitudes fluctuate seasonally. These semiannual variations of nighttime O_3 at northern mid-latitudes, which play a key role in the results presented in this letter, arise from the interplay between annual temperature trends and seasonal H and O variability (Thomas, 1990; Rogers et al., 2009).

The MLT is a difficult region to probe directly as it is too low in altitude for sustained satellite operations and too high for balloon-based techniques; sounding rockets are the unrivaled method for in situ measurements. However, both space- and ground-based instruments are capable of remote O_3 sensing. The Sounding of the Atmosphere using Broadband Emission Radiometry (SABER) instrument aboard the Thermosphere, Ionosphere, Mesosphere Energetics, and Dynamics (TIMED) satellite is one such example, which is the source of the O_3 data used in this work. Mlynczak et al. (2021) have expressed concerns about potential observational gaps in the near future for satellite missions focusing on the chemistry of the MLT, which would be detrimental for fields such as climate monitoring, though alternative observational strategies are possible (e.g. those discussed in Plane et al., 2023). Satellite missions also face an increasing risk of being damaged or destroyed by space junk, recently highlighted by TIMED's near collision (Wall, 2024); in this regard, ground-based methods provide a good alternative.

A microwave radiometry instrument, the Ny-Ålesund Ozone in the Mesosphere Instrument (NAOMI), serves as an example of how MLT O_3 can be detected from the ground. NAOMI relies on a Ku-band (11.072 GHz) rotational transition of $^{16}O_3$; the line shape of this spectrum can be used to reconstruct a vertical O_3 profile (Newnham et al., 2022). Though it lacks the high vertical resolution of satellite instruments, it affords a low-cost method of O_3 monitoring that has shown good agreement with seasonally-averaged SABER data (Newnham et al., 2022). A different, developing technique of ozone estimation relies on the duration distribution of overdense meteor radar echoes. The break point of this power law distribution separates echo durations which are governed by ambipolar diffusion from those affected by chemistry-limited reactions; this inflection value enables computation of O_3 concentration at the corresponding altitude (Jones et al., 1990). Ye and Han (2017) assessed the viability of this approach and found a moderate agreement between meteor-derived O_3 values and satellite observations for the usable altitude range (88–100 km). With additional data and refinement, this technique could enable ozone measurement for 'free' at locations already engaged in meteor radar studies.

The technique presented herein for determining the secondary O_3 vmr maximum is reliant on the fraction of sporadic meteors which exhibit observable optical persistent trains (PTs). The PT phenomenon typically lingers for several minutes after the passage of the meteor, though it can occasionally have a duration exceeding one hour (Beech, 1987). PTs' long-lasting luminosity arises from self-emission via chemiluminescent reactions; chief among these in the visible regime is band emission from excited metal oxides. Jenniskens et al. (1998) suggests iron oxide (FeO) as the primary candidate. FeO is produced in an excited state following the reaction between meteoric Fe and atmospheric O_3

$$Fe + O_3 \rightarrow FeO\left(^5\Delta \text{ etc.}\right) + O_2 \tag{1a}$$
$$FeO + O \rightarrow Fe + O_2 \tag{1b}$$

after which the Fe atom is reclaimed and can participate in additional reactions. A similar reaction can also occur with other common meteoric metals, such as Mg and Ca (Baggaley, 1976). It has been well-documented that PTs occur in a relatively narrow range of altitudes, with average starting and ending heights of ∼95 and 85 km, respectively (Trowbridge, 1907; Yamamoto et al., 2004; Cordonnier et al., 2024)—this is neatly coincident with the range of the secondary O_3 peak. If the majority of enduring PT luminosity arises from emission mechanisms like suggested in reaction 1, then variations in MLT O_3 vmr should directly influence the amount of light produced, which affects how many PTs are sufficiently bright to be detected by camera. Therefore, the observed PT occurrence rate should be reflective of the O_3 content in the MLT region.

2 Data Retrieval

Meteor and PT data were obtained from the Cordonnier et al. (2023a) data set. Briefly, these events were initially recorded by the Widefield Persistent Train Camera 2nd Edition (WiPT2 Cam) which was configured to take long exposure (5 second) images during moonless, nighttime conditions (both moon and sun at least 15° below the horizon). Transient streaks were flagged by a detection pipeline which also filtered out the majority of airplane/satellite trails. The remaining events were then manually reviewed and classified based on the presence of a train; those with trains were further divided into duration bins based on how long the train remained visible, with PTs requiring durations in excess of one minute. Meteors detected by WiPT2 were cross-referenced with the Global Meteor Network (GMN; Vida et al., 2019, 2021), a global network of low-cost CMOS video cameras that record meteors and produce a database of their parameters. Cordonnier et al. (2024) provides complete details on the meteor detection pipeline and subsequent data analyses.

This work incorporates version 2.0 SABER 9.6 μm O_3 data. The custom data tool provided by the SABER team was used to find and retrieve all nighttime events with tangent points occurring within a ±5° latitude and ±5° longitude region centered on the WiPT2 camera (34.3533 N, -106.8851 E) between October 2021 and June 2023. These were additionally filtered to exclude measurements with tangent point solar zenith angles (SZA) less than 105° in order to be consistent with the data collection regime employed by the meteor observations. Since the altitudinal extent of the secondary O_3 maximum aligns quite well with that of the PT zone, we use the peak vmr value of this maximum as a proxy for the total O_3 abundance over the range of pertinent altitudes. To this end, each O_3 vmr profile was interpolated with cubic splines and the maximum value in the range 80 to 105 km was recorded. Multiple O_3 observations occurring in the same orbit within our region of interest were averaged together so as not to create artificial weighting.

3 Results

The impetus for this letter is the good agreement shown by the seasonal variations in the secondary O_3 peak and the variations in observed PT occurrence rates, indicating that the latter can be used as a probe of MLT O_3. We examined this connection on a monthly basis, as this timescale provided enough meteors and O_3 data to be statistically meaningful. The collection of maximum O_3 values for each month were found as described in section 2; their mean value and standard deviation were then calculated. The PT occurrence rate was calculated using only sporadic meteors since they represent a more diverse sampling (e.g. in terms of composition, origin, temporal distribution, etc.) relative to meteors associated with showers. We also enforced a stipulation that the meteor had to end below 93.5 km in order to be included in the rate calculation. This is motivated by the analysis done in Cordonnier et al. (2024); for this particular sample of meteors, those having terminal heights above that altitude did not produce PTs.

We first attempted to relate the PT occurrence rate to the SABER O_3 values using a simple linear relationship, which showed good general agreement, however the corresponding residuals suggested the presence of a moderate time-dependent trend. Kresák (1949) found that the 11-year solar cycle has an effect on the train occurrence rate—during our nearly two year-long campaign, the sun was transitioning from solar minimum toward maximum. These transitional phases correspond to the greatest rate of change in the solar cycle, meaning that PT rates experience the strongest time dependence during these periods. To account for these second-order effects, we incorporated a sinusoidal term into the original linear transformation in order to approximate solar variability. We therefore arrived at the following functional relationship:

$$r_{\mathrm{peak},O_3} = \alpha P + \beta + \gamma \sin\left(\frac{2\pi}{132}(t+55)\right) \tag{2}$$

where r_{peak,O_3} is the monthly average peak O_3 vmr value of the secondary maximum (in ppmv), P is the monthly sporadic PT occurrence rate (in percent), t is the number of months since October 2021, and the Greek coefficients (α, β, γ) are free parameters to be optimized. The simple sinusoidal term assumes a period of 11 years (132 months) and that the last solar minimum occurred in December 2019. The coefficients (α, β, γ) were determined by minimizing the root mean square difference between the SABER O_3 vmr values and the PT-derived values output from Equation 2. These were found to be 0.446, 5.488, and 4.541, respectively. It should be noted that these values are unique to the individual observing equipment and location, as differing camera sensitivities and sky conditions will affect the number of detectable PTs and subsequently the PT occurrence rate.

The preceding results are summarized in Figure 1. Data in the top two panels have been smoothly connected via cubic spline interpolation. The topmost panel shows the monthly PT occurrence rates for sporadic meteors during the entirety of the observing campaign, in which the semiannual variations are readily apparent. The middle panel plots the monthly-averaged peak O_3 vmr of the secondary maximum (from SABER) and the PT-derived O_3 estimate from Equation 2. The gray region indicates the one sigma range of the SABER values. The residuals between the SABER and PT lines are shown in the bottom panel; these are randomly distributed with a mean absolute error of 1.06 ppmv and they do not show any clear time-dependent trends. For the PT-derived O_3 values, 16 of the 21 months (76%) agreed within one sigma of the SABER data, and all 21 agreed within 1.3 sigma. We therefore conclude that Equation 2 does admirably at relating PT rates and O_3 for this two year span of observations—collecting additional data as the solar cycle progresses should both confirm and better constrain the sinusoidal characteristics.

SABER's observations over our region of interest are relatively comprehensive—about 76% of the campaign's duration had an observational gap of three days or less, which increases to 95.2% for intervals of six days or less (the remaining ∼4% is due to two 14-day stretches without observations). Owing to this good coverage, we were able to interpolate the approximate peak O_3 content for each meteor, which enables investigation of ozone's impact on PT production in individual meteor showers. The maximum O_3 vmr for each observation was found as described in section 2. These values were plotted temporally; locally weighted scatterplot smoothing (LOWESS) was applied with a 3% bandwidth. This bandwidth choice maintained a good balance between showing small scale fluctuations while simultaneously reducing the jaggedness of consecutive measurements, which have previously been estimated to have individual uncertainties of ∼20% (Newnham et al., 2022). The smoothed data was interpolated via cubic splines and the O_3 value associated with each meteor's timestamp was determined. The O_3 data for all meteors belonging to the same shower were aggregated and the corresponding mean and standard deviation were calculated. Likewise, the PT occurrence rate for each meteor shower was determined similarly as above, with the same 93.5 km altitude restriction. The results are summarized in Figure 2. Each cyan square relates the average peak O_3 vmr to the PT occurrence rate for a different meteor shower, with error bars showing the one sigma range in O_3. The red circles depict the same quantities, but represent the sporadic meteors occurring in any given month. Linear regression was performed on the sporadic meteor data points; these are described by $P = 1.62 r_{vmr} - 5.37$ where P is the monthly PT occurrence rate for sporadic meteors (in percent) and r_{vmr} is average peak O_3 vmr for those sporadic meteors (in ppmv). The root-mean-square error of this fit is 4.3 percent. To reduce the influence of small sample sizes, Figure 2 only includes meteors showers which produced at least 15 total meteors with 5 or more ending below the altitude cutoff. The data used to create this plot, including the IAU designations of

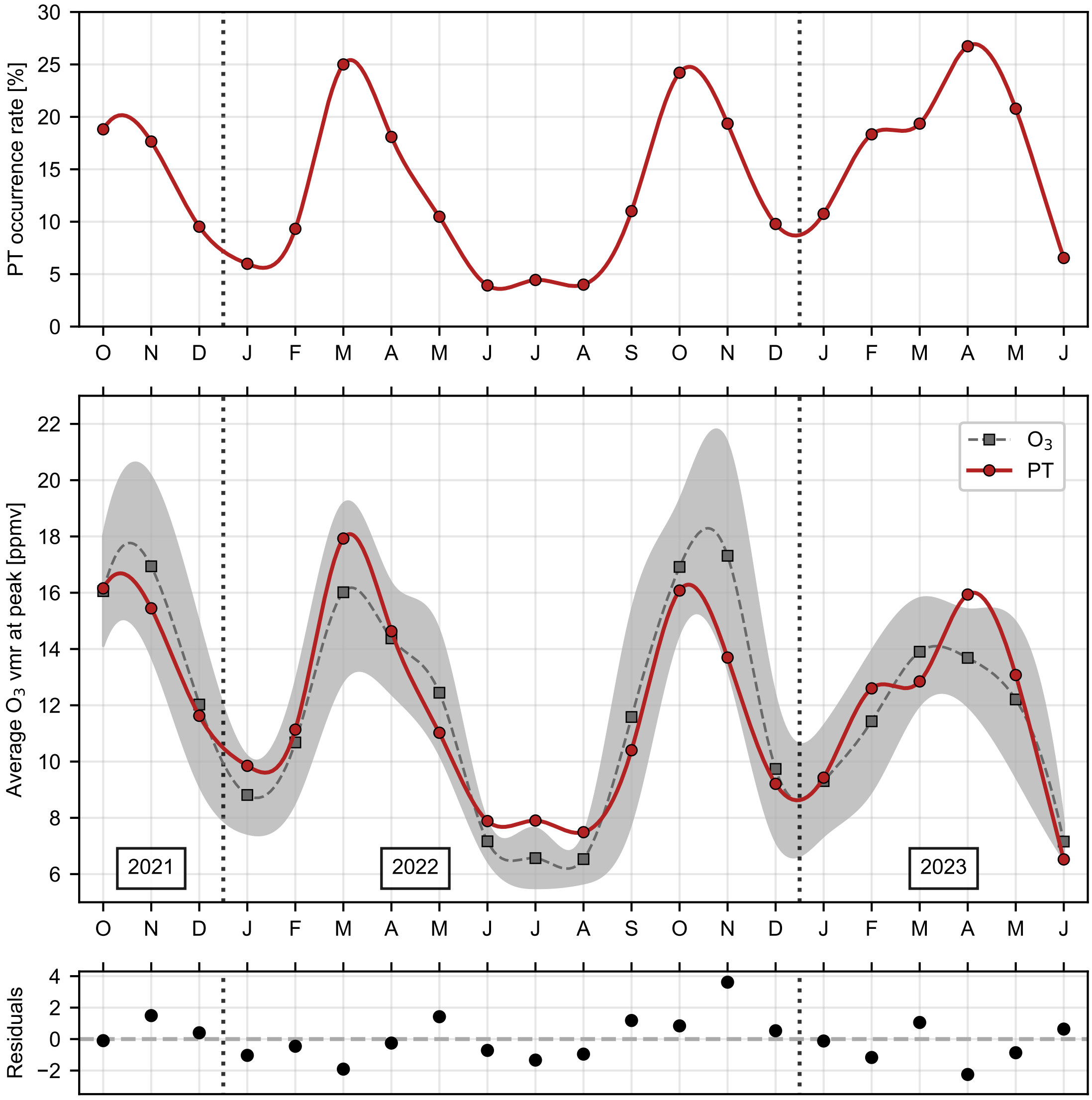

Figure 1. (Top) Monthly PT occurrence rates of sporadic meteors. Data points have been connected via cubic interpolation. (Middle) Connection between the seasonal variations in the peak O_3 vmr of the secondary maximum (averaged monthly) and PT-derived O_3 estimate (from Equation 2). The gray shaded region shows the one sigma range for the monthly O_3 measurements. Data points/error bars have been connected via cubic interpolation. (Bottom) Residuals from the above plot (SABER data minus PT estimate).

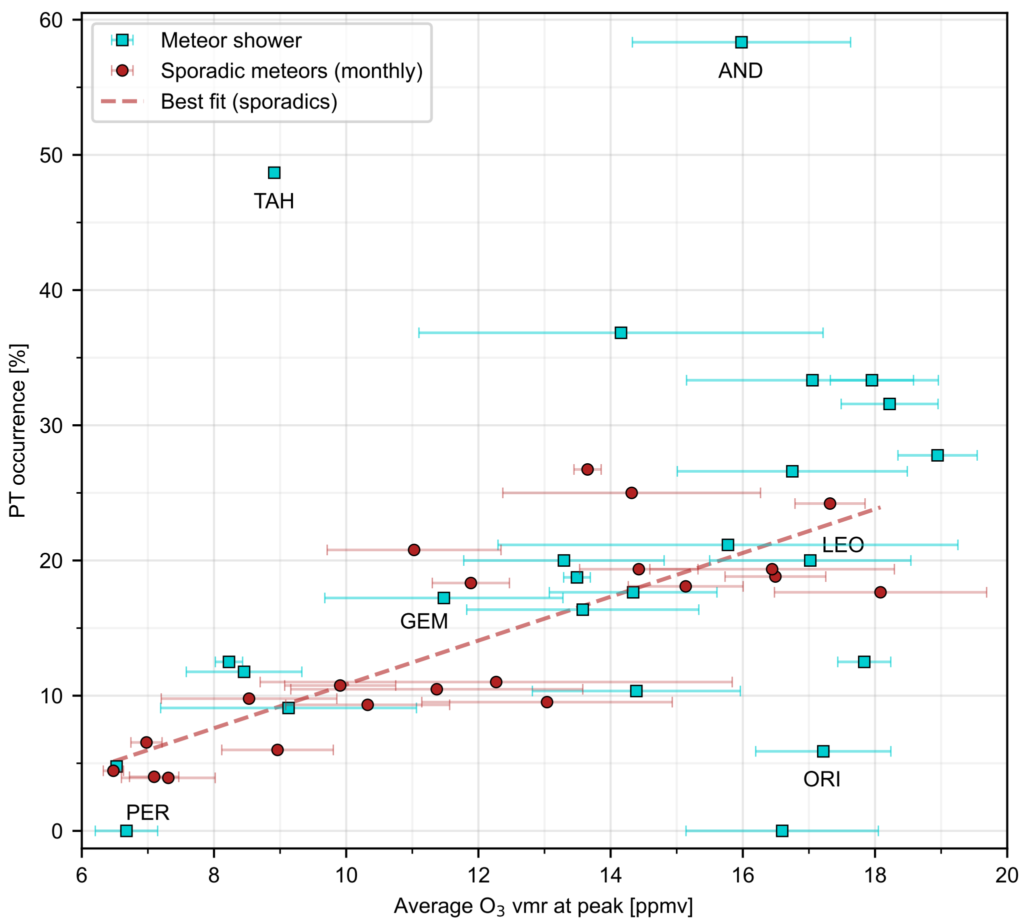

Figure 2. Relationship between the PT occurrence rate for individual meteor showers (cyan squares) and the average peak O_3 vmr encountered by these showers. The peak O_3 vmr was approximated for each meteor in the shower; these values were averaged together to obtain the average peak O_3 vmr depicted by the markers. The sporadic meteors occurring in each month (red circles) are similarly shown. The error bars represent the one sigma range of the individual O_3 values per shower (or month, for the sporadics). Several well-known/interesting meteor showers have been labeled with their IAU three-letter codes, which correspond to the nearest cyan square. The line of best fit for the sporadic meteors is described by $P = 1.62r_{vmr} - 5.37$ (see text for details). It is worth noting the contrast in spread between the PT occurrence rates for shower and sporadic meteors.

the unlabeled showers, can be accessed from the Open Research section. With less than two years' worth of data, we cannot confidently extrapolate the extent to which the solar cycle impacts the PT rate; additional data, ideally from a complete solar cycle, is necessary before attempting to characterize this solar influence. Therefore, we have opted to use the 'raw' PT occurrence rates rather than attempting to apply some manner of normalization factor.

The smoothing and interpolation process is not perfect; in particular, it runs the risk of downweighting or entirely missing small scale night-to-night or transient variations. However, much of this error is mitigated in taking the average value for each meteor shower (which often span weeks or months). Figure 2 shows a clear, strong positive correlation between peak O_3 vmr and PT occurrence rate for sporadic meteors, with a Pearson correlation coefficient of 0.80. Though meteor showers exhibit the same general trend, they have substantially more variability even with high O_3 concentrations (Pearson correlation coefficient of 0.32). Above 14 ppmv O_3, the PT occurrence rate ranges from 0% to nearly 60% for shower meteors, compared to the sporadics which span less than 20% at their broadest. The greater variability among shower meteors almost certainly arises from different intrinsic properties associated with each shower (e.g. composition, dynamical origin, meteoroid strength, etc.). Two showers in particular stand out in Figure 2—the τ-Herculids (TAH) and the Andromedids (AND). Both showers experienced outbursts during our observing campaign, with the TAH outburst occurring in 2022 (Egal et al., 2023) and the AND outburst in 2021 (Jenniskens & Moskovitz, 2022). Nearly all TAH meteors in our data set occurred within several hours of each other, consequently leading to a small one sigma range. The impact of intrinsic meteoroid properties on PT formation, as well as details on the TAH and AND showers specifically, are discussed at length in Cordonnier et al. (2024).

Lastly, the effect O_3 has on PT duration was also investigated. The trains in the original data set had been sorted into custom-width duration bins, with the bin widths being chosen so as to keep the number of trains populating each bin relatively uniform. The peak O_3 vmr for each meteor's train was obtained from the same interpolation method described above. These values were averaged for each duration bin and are plotted in Figure 3 along with their one sigma ranges. Based on this, train duration does not show any clear dependence on O_3 concentration—the greatest difference between mean values is only $\sim$8%. Though the longer duration bins (>5 minutes) have marginally higher O_3 values, the one sigma ranges still overlap comfortably. Cordonnier et al. (2024) found a clear positive correlation between PT duration and meteoroid mass, suggesting that meteoroid mass (or more plausibly, the corresponding meteoric metal content) may play a more significant role than O_3 in determining how long a train endures before fading beyond the detection threshold. The meteoric metal species (e.g. Fe versus Mg, etc.) may also affect the duration and nature of the trains. Other atmospheric considerations (e.g. wind, turbulence, etc.) are all but certain to contribute as well, though a detailed examination of these chemical and dynamical processes is outside the scope of this letter.

4 Discussion

While increased O_3 content more easily facilitates the chemiluminescent reactions, resulting in greater light production and hence easier detectablility, the large spread of PT rates for meteor showers occurring under high O_3 conditions underlines the importance of individual meteoroid properties. Meteoric metal content is expected to have a large influence on PT formation, though factors that affect how those metals are distributed (e.g. meteoroid strength and velocity) will consequently also be significant. Owing to this, the heterogeneity of sporadic meteors reduces the biases associated with meteor showers, making them better suited for estimating O_3. Monthly sporadic meteor counts ranged between 55 and 230 during the campaign, with an average of 130. These counts are sufficiently large to be statistically meaningful, however this does essentially impose a lower

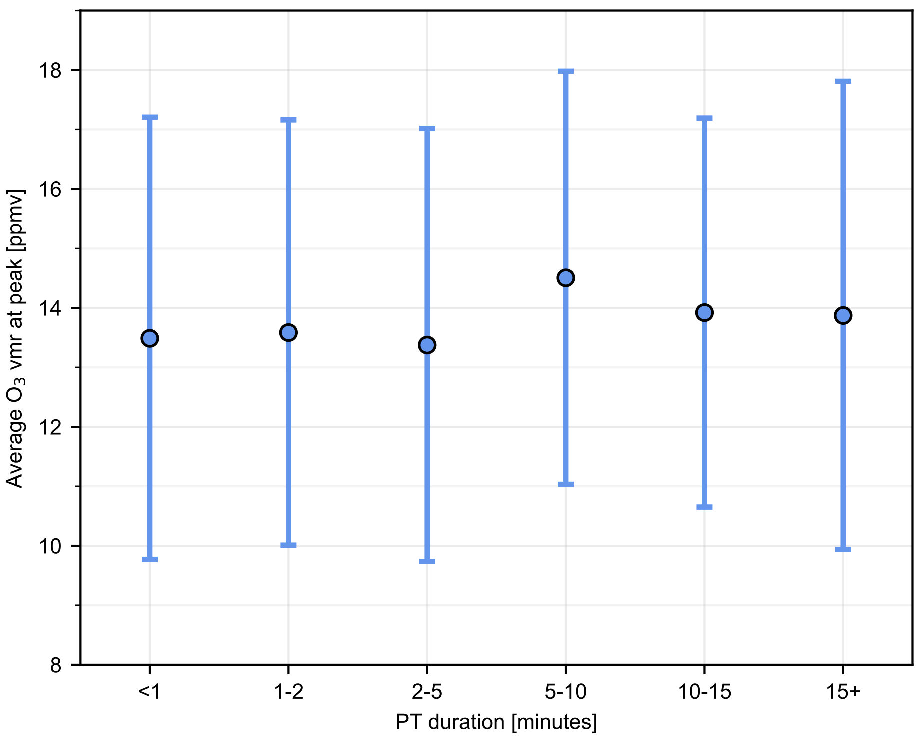

Figure 3. The impact O_3 content has on how long trains last before fading below detection thresholds. The peak O_3 vmr of the secondary maximum was approximated for each meteor in a given duration bin; these values were averaged together to obtain the average peak O_3 vmr for each bin. The error bars show the one sigma range for the individual O_3 values belonging to each bin. No compelling trend can be seen between these quantities.

limit on the temporal resolution of this estimation technique; a single night or perhaps even a week's worth of observations might not produce enough sporadics/PTs to be significant. Additionally, the current WiPT2 observing strategy only records data when the moon is at least 15° below the horizon which further restricts the potential temporal resolution, especially near the full moon phase. Adding other WiPT2-like stations spaced several hundred kilometers apart would increase the number of unique sporadic meteors detected, though this would result in averaging over a substantially larger atmospheric parcel and would still be limited by the same lunar constraint. A WiPT3 camera is also currently under development, which would employ a new fisheye lens capable of capturing four times more light than the WiPT2. In conjunction with these improvements, PT detection software could be developed and deployed for GMN cameras, which would easily expand the global coverage for very little additional cost.

Similarly to the overdense meteor radar echo technique, our method of estimating O_3 is fundamentally limited to the range of altitudes accessible to meteors, more specifically, to the region associated with PTs. Fortunately, this range overlaps with and is nicely localized to the secondary O_3 maximum. We opted to use the peak vmr of this secondary O_3 maximum as our O_3 estimate parameter primarily due to its ease of determination—these values ended up being strongly correlated with the PT occurrence rate. However, a more rigorous treatment of the O_3 data may result in a stronger correlation. For instance, computing the O_3 partial column density or integrating the O_3 vmr over the entire PT altitude range would be more indicative of the total O_3 available to react with the trains. We also attributed the time-dependent nature of Equation 2 to the influence of solar variations on PT rates which, while previously documented and physically motivated, requires long-term observations to fully validate this relation. Collection of additional data over a full solar cycle would go a long way in characterizing both the relationship between PTs and O_3 as well as allowing normalization of PT occurrence rates with respect to solar activity. Interestingly, O_3 is also affected by the solar cycle (e.g. as described in Lee and Wu (2020)), which suggests that the relative impact these variations have on PTs and O_3 differs in severity and/or that these solar effects have a more complicated influence on PTs than simply varying the O_3 concentration.

Regarding Equation 2, our reduction of the solar cycle to a sinusoidal term is a crude approximation; a more rigorous treatment outside the scope of our analysis would instead incorporate actual solar sunspot data. Determination of the α, β, and γ coefficients in Equation 2 also requires calibration from prior O_3 measurements in order to account for the sensitivity of the camera and local sky conditions. This initial calibration necessitates sufficient cotemporal meteor and O_3 measurements which could be challenging without instruments such as SABER. Lastly, classifying whether a given meteor has an observable train is presently done manually via visual inspection, severely limiting this technique's scalability. However, machine learning algorithms are being developed to automatically accomplish this task; this implementation would substantially improve the practicality of this strategy. Though the PT-derived O_3 estimation method introduced in this letter still has several avenues for improvement, it affords a relatively inexpensive (the WiPT2 station cost less than ∼\$6000 in parts) platform for determining O_3 content in the MLT region. This optical meteor train technique could complement existing ground-based microwave (e.g. NAOMI) and radar instruments, with the added benefit of furthering our understanding and population statistics of PTs.

5 Summary

This work demonstrates that the monthly occurrence rates of PTs associated with sporadic meteors are strongly correlated with the peak O_3 vmr of the secondary O_3 maximum. This shows promise as a new, low-cost, ground-based method for monitoring ozone in the MLT, which is traditionally a difficult region to probe. With the suggested improvements and additions, this technique could be a viable complement to existing ground-based O_3 detectors. Though the PT occurrence rates for meteor showers also generally increased with O_3, they exhibited much larger variability relative to the sporadic meteors. This variability arises because the meteoroid properties associated with each shower are quite homogeneous, leading us to conclude that these intrinsic properties have a large impact in determining whether an observable PT forms, instead of being governed solely by O_3. Lastly, we noted that ozone content does not significantly impact how long a given train persists, again supporting the previous notion.

6 Open Research

The original data for the meteors and PTs considered in this letter are located at `https://lda10g.alliance.unm.edu/~pasi/PTs/PT_tables/` (Cordonnier et al., 2023a). Data used to generate the figures and perform the analyses presented herein can be obtained from `https://lda10g.alliance.unm.edu/~pasi/PTs/O3_tables/` (Cordonnier et al., 2023b). GMN meteor data are released under the CC BY 4.0 license, and can be accessed at `https://globalmeteornetwork.org/data/` (Vida et al., 2019, 2021). SABER O_3 data was retrieved from `https://saber.gats-inc.com/` according to the specifications outlined in Section 2. The figures were produced using matplotlib v3.6.2 (`https://matplotlib.org/`; Hunter, 2007). Data were organized and manipulated using pandas v2.0.3 (`https://pandas.pydata.org/`; The pandas Development Team, 2023; McKinney, 2010). Optimization of Equation 2 and data interpolation were both performed using SciPy v1.11.3 (`https://scipy.org/`; Virtanen et al., 2020).

Acknowledgments

The authors thank Ralph Kelly and Jack Hines of Space Dynamics Laboratory for the design and construction of the WiPT2 system, including the automated clamshell sun shield and temperature control system. The authors recognize and thank the GMN station operators whose time and effort enabled the meteor observations used in this work. The authors also appreciate the work that the SABER team put into processing and preparing their data, and for making it easily accessible. L.E. Cordonnier and G.B. Taylor acknowledge support for this research from the National Science Foundation under grant AST-1835400 and from the Air Force Research Laboratory (AFRL). L.E. Cordonnier acknowledges support from an appointment to the AFRL Scholars Program at Kirtland Air Force Base, administered by Universities Space Research Association (USRA) through a contract with AFRL. This research was sponsored in part by the Air Force Office of Scientific Research (AFOSR) Lab Task 23RVCOR002. D. Vida was supported in part by the NASA Meteoroid Environment Office under cooperative agreement 80NSSC21M0073. The views expressed are those of the authors and do not reflect the official guidance or position of the United States Government, the Department of Defense or of the United States Air Force. The appearance of external hyperlinks does not constitute endorsement by the United States Department of Defense (DoD) of the linked websites, or the information, products, or services contained therein. The DoD does not exercise any editorial, security, or other control over the information you may find at these locations.

References

Baggaley, W. J. (1976). The role of the oxides in meteoric species as a source of meteor train luminosity. *Monthly Notices of the Royal Astronomical Society*, *174*, 617-620. doi: 10.1093/mnras/174.3.617

Beech, M. (1987). On the trail of meteor trains. *Quarterly Journal of the Royal Astronomical Society*, *28*, 445.

Cordonnier, L. E., Obenberger, K. S., Holmes, J. M., & Taylor, G. B. (2023a). *Persistent train and associated meteor data* [dataset]. LWA Data Archive. Retrieved from `https://lda10g.alliance.unm.edu/~pasi/PTs/PT_tables/`

Cordonnier, L. E., Obenberger, K. S., Holmes, J. M., & Taylor, G. B. (2023b). *Persistent train and processed ozone data* [dataset]. LWA Data Archive. Retrieved from `https://lda10g.alliance.unm.edu/~pasi/PTs/O3_tables/`

Cordonnier, L. E., Obenberger, K. S., Holmes, J. M., Taylor, G. B., & Vida, D. (2024). Not so fast: A new catalog of meteor persistent trains. *Journal of Geophysical Research: Space Physics*.

Egal, A., Wiegert, P. A., Brown, P. G., & Vida, D. (2023). Modeling the 2022 τ-Herculid outburst. *The Astrophysical Journal*, *949*(2), 96. doi: 10.3847/1538-4357/acb93a

Hunter, J. D. (2007). Matplotlib: A 2D graphics environment. *Computing in Science & Engineering*, *9*(3), 90–95. doi: 10.1109/MCSE.2007.55

Jenniskens, P., Lacey, M., Allan, B., Self, D., & Plane, J. (1998). FeO "orange arc" emission detected in optical spectrum of Leonid persistent train. *Earth, Moon, and Planets*, *82-83*, 429-438. doi: 10.1023/A:1017079725808

Jenniskens, P., & Moskovitz, N. (2022). An outburst of Andromedids on November 28, 2021. *eMeteorNews*, *7*(1), 3-5.

Jones, J., McIntosh, B., & Simek, M. (1990). Ozone and the duration of overdense radio meteors. *Journal of Atmospheric and Terrestrial Physics*, *52*(4), 253-258. doi: 10.1016/0021-9169(90)90092-2

Kresák, L. (1949). On the connection between long-enduring meteor trains and changes of solar activity. *Bulletin of the Astronomical Institutes of Czechoslovakia*, *1*, 87.

Lee, J. N., & Wu, D. L. (2020). Solar cycle modulation of nighttime ozone near the mesopause as observed by MLS. *Earth and Space Science*, *7*(4), e2019EA001063. doi: 10.1029/2019EA001063

McKinney, W. (2010). Data structures for statistical computing in Python. In S. van der Walt & J. Millman (Eds.), *Proceedings of the 9th Python in Science Conference* (p. 56-61). doi: 10.25080/Majora-92bf1922-00a

Mlynczak, M. G., Yue, J., McCormack, J., Liebermann, R. S., & Livesey, N. J. (2021). An observational gap at the edge of space. *Eos*, *102*. doi: 10.1029/2021EO155494

Newnham, D. A., Clilverd, M. A., Clark, W. D. J., Kosch, M., Verronen, P. T., & Rogers, A. E. E. (2022). Ground-based Ku-band microwave observations of ozone in the polar middle atmosphere. *Atmospheric Measurement Techniques*, *15*(8), 2361-2376. doi: 10.5194/amt-15-2361-2022

Plane, J. M. C., Gumbel, J., Kalogerakis, K. S., Marsh, D. R., & von Savigny, C. (2023). Opinion: Recent developments and future directions in studying the mesosphere and lower thermosphere. *Atmospheric Chemistry and Physics*, *23*(20), 13255-13282. doi: 10.5194/acp-23-13255-2023

Rogers, A. E. E., Lekberg, M., & Pratap, P. (2009). Seasonal and diurnal variations of ozone near the mesopause from observations of the 11.072-ghz line. *Journal of Atmospheric and Oceanic Technology*, *26*(10), 2192-2199. doi: 10.1175/2009JTECHA1291.1

Smith, A. K., Harvey, V. L., Mlynczak, M. G., Funke, B., García-Comas, M., Hervig, M., ... Walker, K. A. (2013). Satellite observations of ozone in the upper mesosphere. *Journal of Geophysical Research: Atmospheres*, *118*(11), 5803-5821. doi: 10.1002/jgrd.50445

Smith, A. K., & Marsh, D. R. (2005). Processes that account for the ozone maximum at the mesopause. *Journal of Geophysical Research: Atmospheres*, *110*(D23). doi: 10.1029/2005JD006298

The pandas Development Team. (2023). *pandas-dev/pandas: Pandas* [software]. Zenodo. doi: 10.5281/zenodo.8092754

Thomas, R. J. (1990). Atomic hydrogen and atomic oxygen density in the mesopause region: Global and seasonal variations deduced from Solar Mesosphere Explorer near-infrared emissions. *Journal of Geophysical Research:*

Atmospheres, *95*(D10), 16457-16476. doi: 10.1029/JD095iD10p16457

Trowbridge, C. C. (1907). Physical nature of meteor trains. *The Astrophysical Journal*, *26*(2), 191-205. doi: 10.1086/141478

Vaughan, G. (1982). Diurnal variation of mesospheric ozone. *Nature*, *296*(5853), 133-135. doi: 10.1038/296133a0

Vida, D., Gural, P. S., Brown, P. G., Campbell-Brown, M., & Wiegert, P. (2019). Estimating trajectories of meteors: an observational Monte Carlo approach – I. Theory. *Monthly Notices of the Royal Astronomical Society*, *491*(2), 2688-2705. doi: 10.1093/mnras/stz3160

Vida, D., Šegon, D., Gural, P. S., Brown, P. G., McIntyre, M. J. M., Dijkema, T. J., … Zubović, D. (2021). The Global Meteor Network – Methodology and first results. *Monthly Notices of the Royal Astronomical Society*, *506*(4), 5046-5074. doi: 10.1093/mnras/stab2008

Virtanen, P., Gommers, R., Oliphant, T. E., Haberland, M., Reddy, T., Cournapeau, D., … SciPy 1.0 Contributors (2020). SciPy 1.0: Fundamental algorithms for scientific computing in Python. *Nature Methods*, *17*, 261–272. doi: 10.1038/s41592-019-0686-2

Wall, M. (2024, February 28). *Near miss! NASA satellite, dead Russian spacecraft zoom past each other in orbit.* Space.com. `https://www.space.com/near-collision-nasa-timed-satellite-russian-space-junk`.

Yamamoto, M.-Y., Toda, M., Higa, Y., Maeda, K., & Watanabe, J.-I. (2004). Altitudinal distribution of 20 persistent meteor trains: Estimates derived from Metro campaign archives. *Earth, Moon, and Planets*, *95*(1-4), 279-287. doi: 10.1007/s11038-005-9048-4

Ye, Q.-Z., & Han, S. X. (2017). Ozone measurements with meteors: A revisit. *Monthly Notices of the Royal Astronomical Society*, *472*(1), 2-7. doi: 10.1093/mnras/stx1851